INFLUENCE OF THE PROBE GEOMETRICAL FEATURES ON THE STRESS CONDITION OF THE TOOL DURING FRICTION STIR WELDING

I. GOLUBEV*'**, M. WEIGL* and V. MICHAILOV**

*Grenzebach Maschinenbau GmbH, 86663 Asbach-Bäumenheim, Hamlar, Germany, Iurii.Golubev@grenzebach.com
**Brandenburg University of Technology (BTU) Cottbus-Senftenberg, 03046 Cottbus, Germany

DOI 10.3217/978-3-85125-615-4-34

ABSTRACT

The objective of the present paper is to investigate the effect of the tool probe features on the stress condition of the tool in friction stir welding (FSW). The friction stir welding of an Al 6082 T6 alloy was performed to provide validation data for numerical models of the process. The developed earlier 3D thermal model was improved in order to collect the data about workpiece material strength and heat generation at the probe/workpiece interface during FSW. These data were used as a boundary conditions in models for temperature in the welding tool and stress condition of the tool. Influence of temperature and tool probe features such as flat depth, thread root radius and probe root radius, on stress condition of FSW tool at different angular position was defined.

Keywords: Friction Stir Welding, Aluminum Alloys, Numerical Simulation, Stress Analysis, Probe Geometry

INTRODUCTION

Friction stir welding (FSW) is the solid-state joining technique invented in 1991 by TWI. The FSW method have a number of advantages over conventional methods of fusion welding such as no solidification cracks, low distortion and low residual stresses in the workpiece. However, the method has some disadvantages. One of the main disadvantages is the slower welding speed of the process compared to the competing welding processes.

An increase of the welding speed can result in insufficient material flow around the tool probe leading to the defects formation such as void or lack of fill [1-2]. Numerous researchers tried to enhance the material flow through the improvement of the tool probe geometry [3-15]. They used various outer shape of the probe [9-10, 13], thread [3-8, 11-13, 15] and addition of machined flats or flutes on the tool probe [3-6, 12, 14-15]. Thomas et al. [3] concluded that the existence of thread and flutes aids material flow because of swept ratio increase. It is this ratio of the 'dynamic volume' of the tool to the static volume of the

tool that is important in providing an adequate flow path. Fujii et al. [6] showed that a profiled tool probe can provide a sound weld even at a relative high welding speed.

The welding tool is heavily loaded during FSW process due to high temperature gradient [8-16] and interaction of the tool surfaces with workpiece material. The tool probe geometrical features enhancing the material flow can become the weak points leading to the earlier tool breakage. Some researchers [3, 15] calculated numerically the stresses in the FSW tools under the same loading conditions to compare the tools of different designs. Thomas et al. [3] applied uniform pressure loads to the faces of the tool to create pure torsion, pure bending and combination of the two loading modes. Reza-E-Rabby [15] defined the stress distributions in the FSW tool by applying experimentally measured loads to the faces of the tool probe and determined that the maximum von Mises stress is observed at a point where there is full thread depth closest to the tool shank. The pressure load distributed over the tool surfaces is influenced by the temperature-dependent flow stress of the workpiece material. Experimental measurements of the temperature in the weld nugget are difficult to achieve, but numerical simulation enables to determine the temperature and, therefore, the material flow stress and pressure load.

The objective of the present work is to develop the model that predicts the stresses in the FSW tool from the mechanical and thermal properties of the tool and workpiece materials, the tool and workpiece dimensions and the process parameters. The temperature data is collected to enable model to be validated. The developed model is used to investigate the influence of the probe geometrical features on the stress condition of the welding tool. Furthermore, a new welding tool with improved probe geometry is proposed.

EXPERIMENTAL PROCEDURE

MATERIAL

In this work plates of 6082 – T6 aluminium alloy with the dimensions 300 × 75 × 3 mm have been welded with FSW. The chemical composition and mechanical properties of the aluminium alloy used in the experiments are given in Table 1 and Table 2, respectively.

Table 1 Nominal chemical composition of the workpiece material AA 6082 T6

Si	Fe	Cu	Mn	Mg	Al
0.89	0.4	0.31	0.4	1.18	Bal.

Table 2 Mechanical properties of the workpiece material AA 6082 T6

Ultimate tensile strength, MPa	Yield strength, MPa	Elongation, %
323	256,8	6,3

WELDING TRIALS

Temperature measurements were carried out during FSW using thermocouples placed on the top surface of the weld plates to validate the calculated results. To ensure repeatability, three welds were successfully replicated, showing nearly identical temperature histories. Figure 1 shows the thermocouples position during the FSW process.

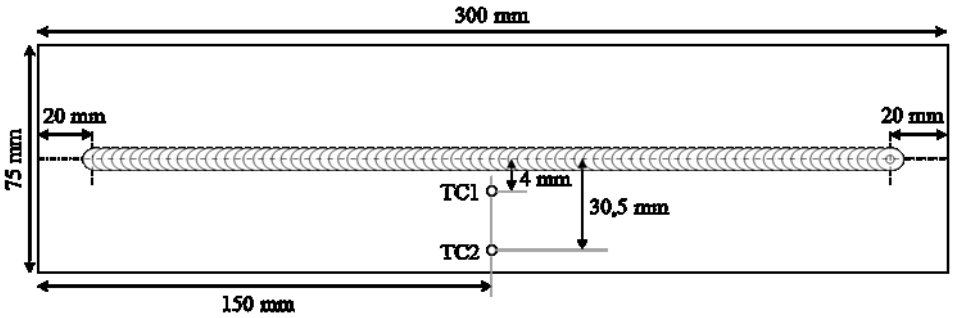

Fig. 1 Thermocouples position

The experiments were carried out on a force-controlled robotic FSW system by Grenzebach Maschinenbau GmbH (Germany) employed with a heavy-duty robot KUKA KR5000 and a specially designed spindle for rotational speeds up to 14000 rpm. For the FSW process a conventional welding tool made of WC-10Co alloy was used. The welding tool consisted of a threaded tapered probe with a 3 mm root diameter, 2,2 mm tip diameter and a 2,3 mm length and a flat shoulder with a 5,5 mm diameter. The welding tool features were three flats with depth of 0,3 mm, thread with thread root radius of 0,14 mm and probe root radius of 0,3 mm. The rotational speed, traverse speed, axial force and tilt angle were set to the constant values of 2500 RPM, 1000 mm/min, 3 kN and 3° respectively.

MODELLING OF FRICTION STIR WELDING

THERMAL MODELLING

The thermal modelling process is divided into two steps. The first step is the calculation of the temperature in the workpiece and total heat generation at the tool/workpiece interface by using 3-dimensional finite element model with the analytical heat source model moving along the weld line. The second step is the 3-dimensional finite element model uses calculated heat generation at the tool/workpiece interface as boundary condition for the calculation of the temperature distribution in the welding tool.

The calculation of the temperature in the welding tool were performed for 7 welding tools having different geometrical features such as flat depth, probe root radius and thread root radius. The varied geometrical features are shown in Table 3.

Table 3 Varied geometrical features

Flat depth, mm	Probe root radius, mm	Thread radius, mm
0,25	0,2	0,14
0,3	0,3	0,16
0,35	0,35	0,18

In this work, it is assumed that change of the probe geometrical features has no significant influence on the heat generation at the tool/workpiece interface and temperature in the weld nugget. Hence, the heat generation calculated in the first model for the initial welding tool is used for the calculation of the temperature distribution in all welding tools.

Analytical heat source model

The heat source model is the distribution of the local heat generations at the contact interface between the welding tool and workpiece. The local heat generation at the interface segment is given by

$$q = \tau_{contact}\omega r \tag{1}$$

where ω is the angular velocity, r is the distance from the interface segment to the rotational axis and τ is the contact shear stress at the contact interface equals the yield shear stress τ_{yield} and can be converted from experimentally measured yield stress data using the following expression

$$\tau_{contact} = \tau_{yield} = \frac{\sigma_{yield}}{\sqrt{3}} \tag{2}$$

where σ_{yield} is the yield stress depending on the temperature of the workpiece material at the contact interface.

By integration the equation (1) over the shoulder, probe side and probe tip surfaces are found total heat generations at the shoulder $Q_{shoulder}$, probe side $Q_{probe\ side}$ and probe tip $Q_{probe\ tip}$ respectively. The total heat generation over the entire contact interface between the welding tool and workpiece is given by

$$Q_{total} = Q_{shoulder} + Q_{probe\ side} + Q_{probe\ tip} \tag{3}$$

The heat generated at the contact interface flows into the both the welding tool and the workpiece. The thermal efficiency η describes how much heat is conducted into the workpiece itself compared to the total heat generation Q_{total}. The heat conducted in the workpiece $Q_{workpiece}$ is given by

$$Q_{workpiece} = \eta Q_{total} \tag{4}$$

The heat conducted in the welding tool is given by

$$Q_{tool} = (1 - \eta)Q_{total} \tag{5}$$

The thermal efficiency can be calculated by using thermophysical properties of the workpiece and tool materials [Chen, Feng 2016], i.e.

$$\eta = \frac{\sqrt{(\lambda\rho C_p)_W}}{\sqrt{(\lambda\rho C_p)_W + (\lambda\rho C_p)_T}} \tag{6}$$

Where λ is the thermal conductivity, ρ is the density, C_p is the heat capacity, the subscripts W and T denote the workpiece and tool, respectively.

Finite element model for the temperature and heat generation

Figure 2 shows the finite element model for the temperature in the workpiece and the total heat generation at the tool/workpiece interface.

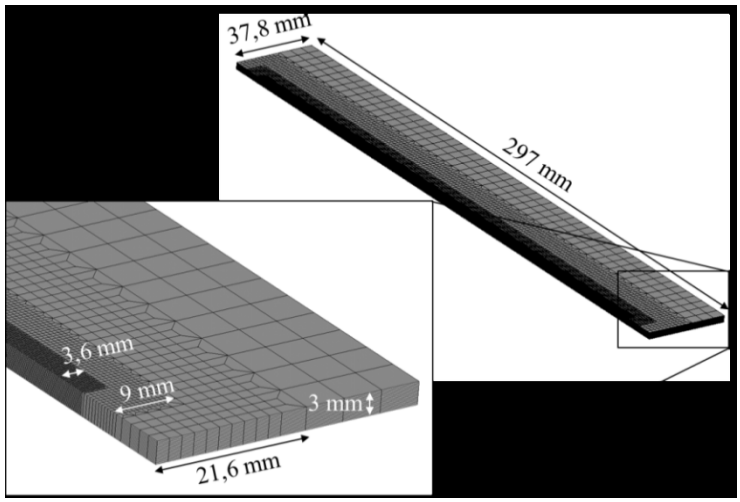

Fig. 2 Finite element model for the temperature and heat generation

In this work, it is assumed that two plates are welded symmetrically and the heat generation is symmetrical about the welding line. Thus only one plate is modelled. The welding tool and backing plate are not included in the calculation to limit the number of the geometries that are enmeshed and save computational resources. Enmeshed model consists of 642590 hexahedral elements with a single degree of freedom, temperature. The mesh

density is varied over the width of the workpiece model. The higher mesh density is near the welding line where the higher temperature gradient is expected.

The effect of the backing plate is taken into account due to application of a temperature-dependent equivalent heat transfer coefficient at the bottom surface of the workpiece h_{bp} given in Table 4. The welding tool is modelled by applying of the heat flux to the contact interface between the tool and workpiece. The heat flux is described by equation (1) requiring temperature-dependent yield shear stress data given in Table 5. Convective heat loss to the air is applied at the top and side surfaces of the workpiece using a temperature-dependent convective heat transfer coefficient α_{tool} given in Table 6.

Table 4 Equivalent heat transfer coefficient, °C / × 10^{-5} W mm^{-2} K^{-1}

20	40	50	100	200	500
3,9	4,9	7,7	8,5	11	65

Table 5 Yield shear stress data, °C / MPa

20	100	200	300	370	420	500	630
158	150	130	58	29	12	6	0

Table 6 Convective heat transfer coefficient, °C / × 10^{-5} W mm^{-2} K^{-1}

20	100	200	300	400	500
2,5	2,722	3,143	3,729	4,508	5,511

Finite element model for the temperature in the welding tool

Figure 3 illustrates the geometrical model and boundary conditions of the model for the temperature distribution in the welding tool.

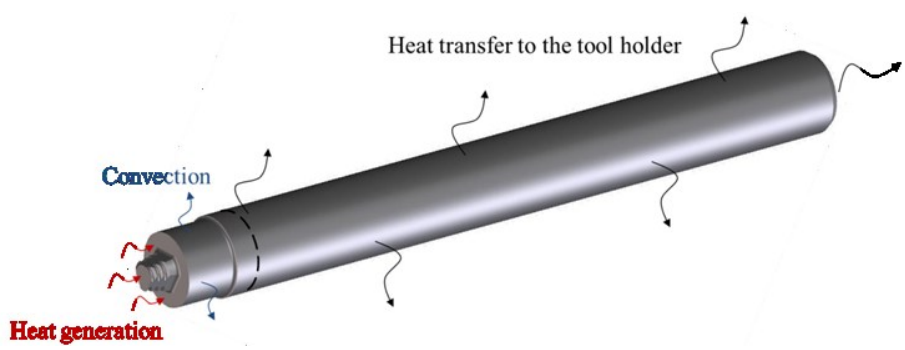

Fig. 3 Schematic illustration of boundary conditions for the thermal analysis of the welding tool

For the thermal characteristics of the considered WC-10Co alloy, the following values were utilized: thermal conductivity λ = 0,11 W mm^{-1} K^{-1}, density ρ = 14,5 g cm^{-3} and thermal capacity c = 0,134 J g^{-1} K^{-1}. The heat loss is realized through the convection to the air and heat transfer to the tool holder from the shank surfaces. Convective heat transfer coefficient α_{tool} = 25 × 10^{-6} W mm^{-2} K^{-1} was applied at the shank surface between the tool shoulder and dotted line as shown in Figure 3. The effect of the tool holder was taken into account due to application of an equivalent heat transfer coefficient h_{th} = 10^{-3} W mm^{-2} K^{-1} at the shank surface in contact with the tool holder (above the dotted line).

The geometrical models of 7 welding tools were enmeshed with the mesh density varied over the height of the tool model. The higher mesh density was at the tool probe and shoulder where the higher temperature gradient is expected. The smallest element edge length was 0,04 mm.

The total heat generation at the shoulder and tool probe surfaces was defined in the first model for temperature in the workpiece. The fraction of the total heat conducted into the FSW tool was calculated by equation (5).

MODELLING OF THE STRESSES IN THE TOOL

The modelling process of stresses in the welding tool is also divided into two steps. The first step is a structural analysis evaluating stresses due to temperature distribution in the welding tool. The second step is the model uses thermal stresses as initial condition for the model when subjected to a load due to interaction with the workpiece material.

The calculation of the stresses in the welding tool were also performed for 7 welding tools having different geometrical features.

Thermal-stress analysis

Figure 4 illustrates the geometrical model and boundary conditions for the thermal-stress analysis.

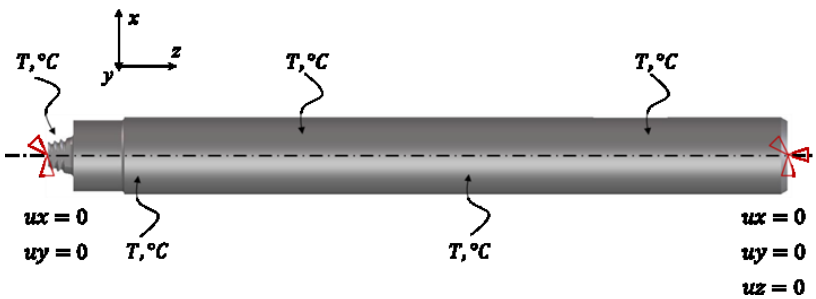

Fig. 4 Schematic illustration of the boundary conditions for the thermal stress analysis

The following characteristics of WC-10Co alloy were used in the numerical model for stresses: coefficient of thermal expansion α = 5,5 × 10^{-6} °C^{-1}, Young's modulus E = 580

GPa and Poisson ration v = 0,3.The results of the model for the temperature distribution in the welding tool are converted to a temperature load for the thermal-stress analysis of the welding tool.

Stress analysis

Interaction of the welding tool with the workpiece material results in reaction forces that the tool experiences during the FSW process. While the rotation of the welding tool causes the torsional forces at the entire tool/workpiece contact interface, the tool traverse affects the traverse forces acting on the leading side of the tool probe, as shown in Figure 5.

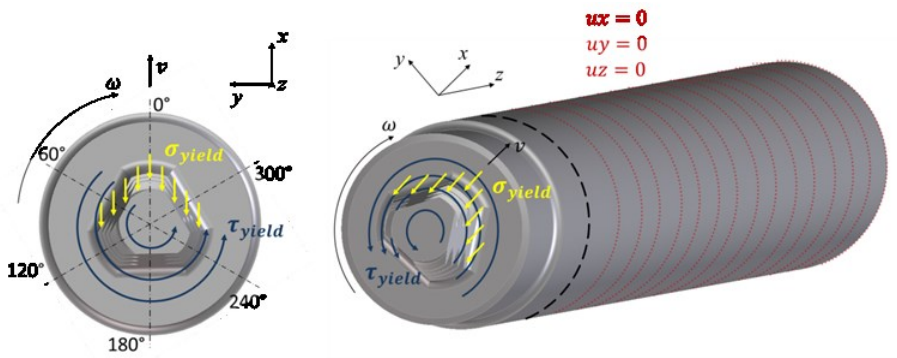

Fig. 5 Schematic illustration of the boundary conditions for the stress analysis in the tool

The plastic deformation of shear layer contacting the welding tool is the necessary condition for the successful weld. Hence, the traverse and torsional forces can be represented as pressure corresponding to workpiece material yield strength and shear yield strength respectively. The yield strength and shear yield strength of the workpiece material depend on the temperature and can be defined by means of calculation results of the model for the temperature in the workpiece described before.

The tool probe is not axisymmetric because of helical nature of the thread. Hence, it is necessary to load the tool probe from different direction in order to define the weak angular position. Six different orientations were chosen, as shown in Figure 5.

RESULTS AND DISSCUSSIONS

HEAT INPUTS AND TEMPERATURE DISTRIBUTION

Figure 6 shows the comparison between numerically estimated and experimentally measured temperature cycles on the top surface of the workpiece during FSW.

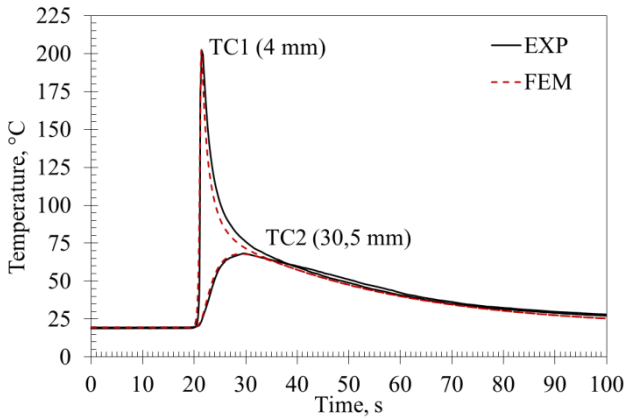

Fig. 6 Comparison between numerical and experimental temperature cycles

The computed temperature cycles are in good agreements with the experimental measurements. Therefore the model can be used to calculate the heat generation at the tool/workpiece interface and temperature in the weld nugget.

The calculated heat generations at different tool surfaces conducted in the workpiece and conducted in the welding tool are given in Table 7.

Table 7 Calculated heat generations at different tool surfaces during steady-state FSW

Heat generation	Shoulder	Probe side	Probe tip
Total, W	312,5	182,5	32,5
Workpiece, W	287,5	167,9	29,9
Tool, W	25	14,6	2,6

The calculated heat generation over the entire contact interface between the welding tool and workpiece is found to be 527,5 W. The most of the heat (59 %) is generated at the shoulder/workpiece interface, while the heat fractions of 35 % and 6 % are generated at the probe conical side and probe tip respectively.

Figure 7 shows the calculated temperature distribution in the workpiece during the steady-state FSW process.

Since most of the heat is generated at the shoulder/workpiece interface, the workpiece temperature decreases from the tool shoulder to the probe tip. It is also observed that the workpiece temperature under the leading side of the welding tool is lower than under the tool trailing side because of welding tool traverse. The temperature of the workpiece material being in contact with the welding tool is found to be not uniform. Hence the pressure loads distributed over the tool surfaces is not uniform. The calculated maximum temperature of 421 °C is observed on the workpiece top surface under the trailing side of the tool shoulder. The calculated lowest temperature of 296 °C is observed on the leading edge of the tool probe tip.

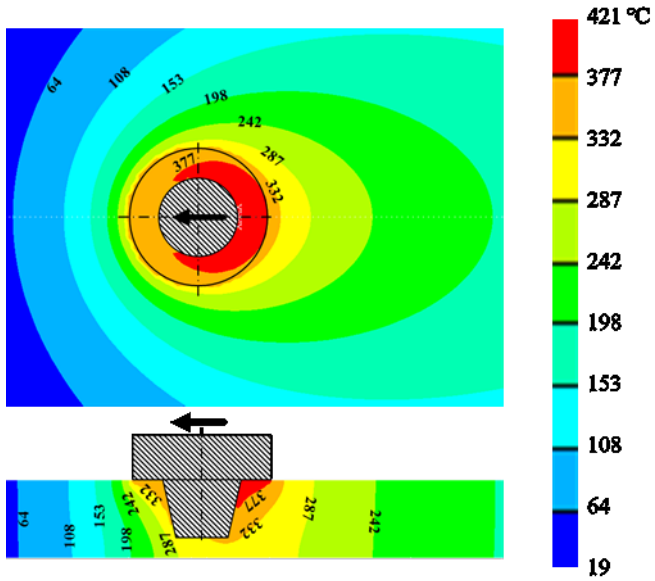

Fig. 7 Temperature distribution in the workpiece during steady-state FSW

Figure 8 shows the calculated temperature distribution in the initial welding tool with flat depth of 0,3 mm, probe root radius of 0,3 mm and thread root radius of 0,14 mm during the steady-state FSW process.

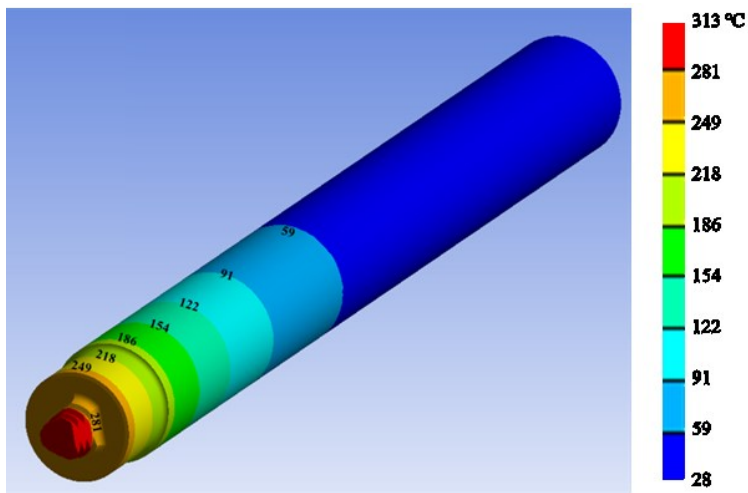

Fig. 8 Temperature distribution in the welding tool of initial geometry

The temperature distributions in the FSW tool is not uniform over the welding tool height. The temperature decreases from probe tip to the end face of the tool shank because of heat generation on the tool probe and shoulder and high heat transfer from the tool shank

surfaces to the tool holder. The calculated maximum temperature of 313 °C is observed on the tool probe tip. The minimum temperature of 28 °C is observed on the end edge of the tool shank. The lowest temperature of the tool surface being in contact with the workpiece is found to be 254 °C.

STRESS CONDITION OF THE TOOL

Figure 9 shows the calculated thermal stresses in the initial welding tool with flat depth of 0,3 mm, probe root radius of 0,3 mm and thread root radius of 0,14 mm during the steady-state FSW process.

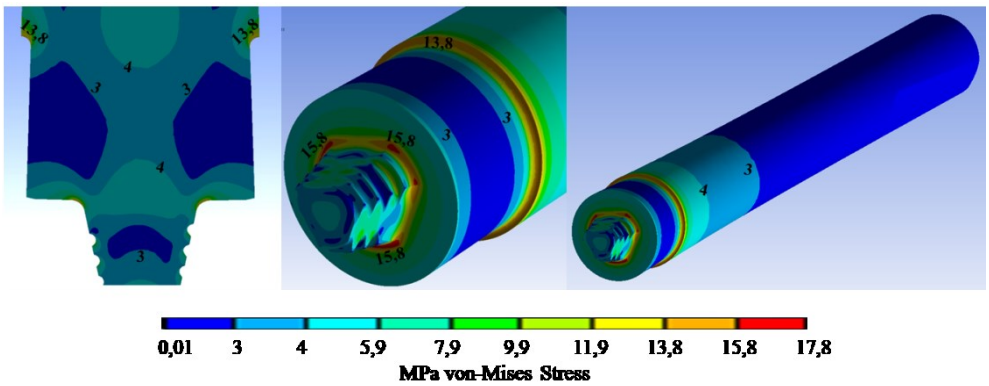

Fig. 9 Thermal stresses in the welding tool of initial geometry

The calculated maximum stress of 17,8 MPa is observed at the probe root. Since the maximum stress due temperature distribution is found to be much less than the tool material strength, the welding tool breakage cannot be caused by thermal stress only.

Figure 10 shows influence of the tool angular position on maximum von Mises stress resulted by combination of temperature load and interaction with the workpiece material.

The angular position of 300 deg. is found to be the critical orientation having maximum stress of 949 MPa. Hence the welding tool fracture at the angular position of 300 deg. is expected. The lowest maximum stress of 864 MPa is observed at the tool angular position of 180 deg. The weak point is observed on the thread root being closest to the tool shoulder at the advancing side for all loading orientation.

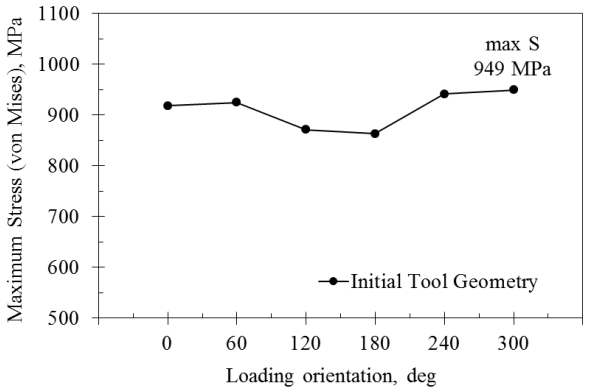

Fig. 10 Maximum stress for different loading orientation of welding tool

The stress distributions in the welding tool of initial geometry at the angular position of 300 deg. is shown in Figure 11.

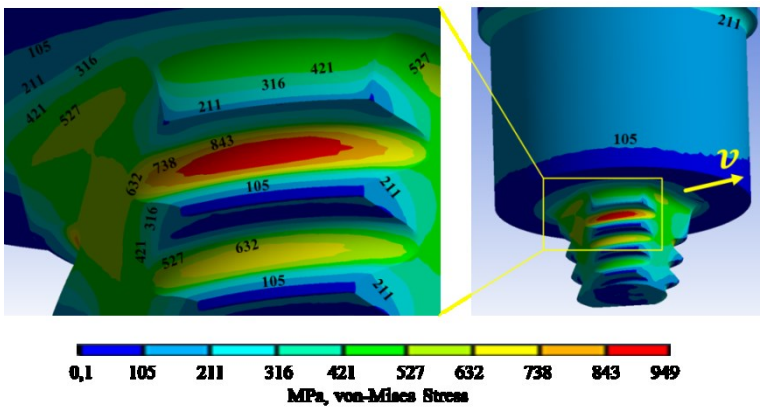

Fig. 11 Stress distributions of initial welding tool at the angular position of 300 deg

The probe conical surface can be divided into six surfaces, three threaded and three flat surfaces. The higher thread is found to weak point for each threaded surface while probe root is found to be weak point for each flat surface. The fracture line can be drawn by connection of the weak points defined on the each surface.

INFLUENCE OF THE PROBE FEATURES ON THE STRESS CONDITION

Figure 12 shows the calculated maximum stress for the welding tools with different flat depth.

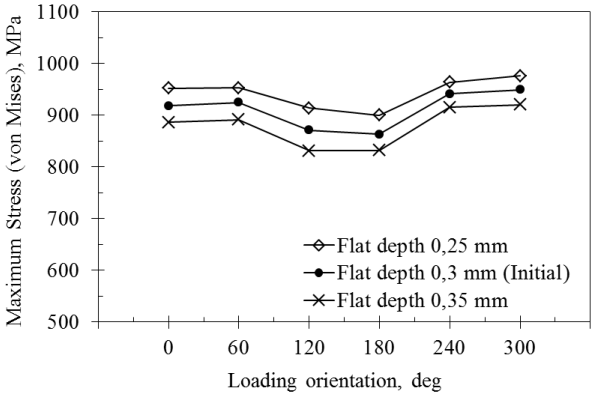

Fig. 12 Influence of flat depth on the stress condition of the welding tool

An increase of the flat depth does not result in the change of the critical orientation. It is observed that increase of the flat depth leads to decrease of maximum stress due to decrease of threaded probe surface being a weak point. Moreover, the flat depth increase causes the increase of the swept ratio and therefore enhances the material flow. However, it is expected that further increase of flat depth can result in increase of maximum stress because of decrease of probe cross-sectional area.

Figure 13 shows the calculated maximum stress for the welding tools with different probe root radius.

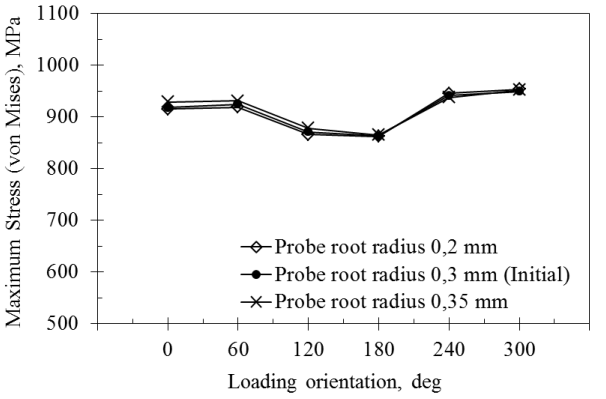

Fig. 13 Influence of probe root radius on the stress condition of the welding tool

Since the weak point is on the thread root, the change of probe root radius has no significant influence on the maximum stress. However decrease of probe root radius results in increase of the stress on the probe root. Hence too small probe root radius can became a weak point and changes the critical orientation of the welding tool.

Figure 14 shows the calculated maximum stress for the welding tools with different thread root radius.

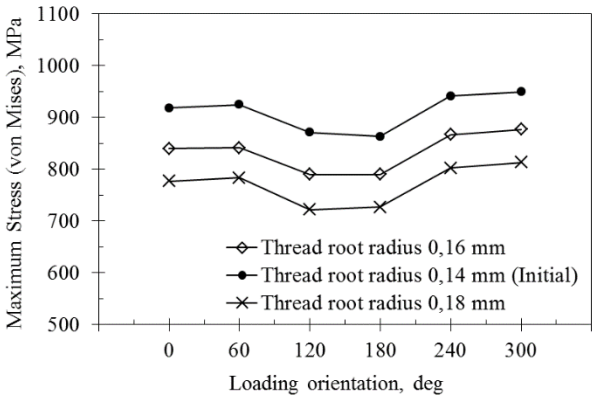

Fig. 14 Influence of thread root radius on the stress condition of the welding tool

An increase of thread root radius does not cause the change of the critical orientation. It is observed that increase of thread root radius results in decrease of maximum stress. Increase of thread root radius causes the decrease of the swept ratio and can lead to insufficient stirring of the workpiece material and therefore weld imperfections (lack of fill).

CONCLUSIONS

A numerical FE model was developed to simulate the stresses in the FSW tool from the mechanical and thermal properties of the tool and workpiece materials, the tool and workpiece dimensions and the process parameters. The model takes into account temperature gradient in the welding tool and not uniform pressure distribution at the tool surfaces. The experimental measurements of process forces and torque are not required.

The model was used to investigate the influence of tool probe geometrical features on the stress condition of the welding tool. The following conclusions can be drawn from the investigation:

The temperature gradient in the welding tool during the FSW has no significant influence on the tool stress condition because of too low maximum thermal stress.

The weak point for each angular position is the highest thread root at the advancing side.

It is expected that the fracture line will go through the higher threads at the threaded probe surfaces and the probe roots at the flat surfaces.

An increase of flat depth results in decrease of maximum stress due to decrease of threaded probe surfaces.

Change of probe root radius has no significant influence on the maximum stress. However decrease of probe root radius causes the increase of stress on the probe root. Hence too small probe root radius can became a weak point.

An increase of thread root radius results in decrease of maximum stress.

It is suggested the combination of higher flat depth with increased thread root radius to decrease the maximum stress.

REFERENCES

[1] A. J. LEONARD and S. A. LOCKYER: 'Flows in friction stir welds', *Proc. Of the 4th International Conference on Friction Stir Welding*, Park City, Utah, USA, 2003.

[2] Y. G. KIM, H. FUJII, T. TSUMURA, T. KOMAZAKI and K. NAKATA: 'Three defect types in friction stir welding of aluminium die casting alloy', *Material Science and Engineering A*, Vol. 415, pp. 250-254, 2006.

[3] W. M. THOMAS, E. D. NICHOLAS and S. D. SMITH: 'Friction stir welding – tool developments', *TMS Annual Meeting*, New Orleans, Louisiana, USA, 2001.

[4] S. W. KALLEE, E. D. NICHOLAS and W. M. THOMAS: 'Friction stir welding – invention, innovations and applications', *INALCO 2001 8th International Conference on Joints in Aluminium*, Munich, Germany, 2001.

[5] R. ZETTLER, S. LOMOLINO, J. F. DOS SANTOS, T. DONATH, F. BECKMANN, T. LIPMANN and D. LOHWASSER: 'A study of material flow in FSW of AA2014-T351 and AA6065-T4 alloys', *Proc. 5th International Conference on Fricition Stir Welding*, Metz, France, 2004.

[6] H. FUJII, L. CUI, M. MAEDA and K. NOGI: 'Effect of tool shape on mechanical properties and microstructure of friction stir welded aluminium alloys', *Material Science and Engineering A*, Vol. 419, pp. 25-31, 2006.

[7] MD. REZA-E-RABBY and A. P. REYNOLDS: 'Effect of tool pin thread form on friction stir weldability of different aluminium alloys', *Procedia Engineering*, Vol. 90, pp. 637-642, 2014.

[8] N. DIALAMI, M. CERVERA, M. CHIUMENTI, A. SEGATORI and W. OSIKOWICZ: 'Experimental Validation of an FSW Model with an Enhanced Friction Low: Application to a Threaded Cylindrical Pin Tool', *Metals*, Vol. 7, No. 491, 2017.

[9] M. A. HUSSAIN, N. Z. KHAN, A. N. SIDDIQUEE and Z. A. KHAN: 'Effect of different tool pin profiles on the joint quality of friction stir welded AA6063', *Materials Today: Proceedings*, Vol. 5, pp. 4175-4182, 2018.

[10] P. GOEL, A. N. SIDDIQUEE, N. Z. KHAN, M. A. HUSSAIN, Z. A. KHAN, M. H. ABIDI and A. AL-AHMARI: 'Investigation on the Effect of Tool Pin Profiles on Mechanical and Microstructural Properties of Friction Stir Butt and Scarf Welded Aluminium Alloy 6063', *Metals*, Vol. 8, No. 74, 2018.

[11] G. CHEN, H. LI, G. WANG, Z. GUO, S. ZHANG, Q. DAI, X. WANG, G. ZHANG and Q. SHI: 'Effect of pin thread on the in-process material flow behaviour during friction stir welding: A computational fluid dynamics study', *International Journal of Machine Tools and Manufacture*, Vol. 124, pp. 12-21, 2018.

[12] MD. REZA-E-RABBY, W. TANG and A. P. REYNOLDS: 'Effect of tool pin features on process response variables during friction stir welding of dissimilar aluminium alloys', *Science and Technology of Welding and Joining*, Vol. 20, No. 5, pp. 425-432, 2015.

[13] F. Y. ISUPOV, A. A. NAUMOV, O. V. PANCHENKO, L. A. ZHABREV and A. A. POPOVICH: 'Comparative analysis of the mechanical properties of aluminium alloys welded joints obtained by friction stir welding', *Proc. Material Science and Technology Conference and Exhibition 2018*, In press.

[14] P. A. COLEGROVE and H. R. SHERCLIFF: 'Two-dimensional CFD modelling of flow round profiled FSW tooling', *Science and Technology of Welding and Joining*, Vol. 9, No. 6, pp. 483-492, 2004.

[15] MD. REZA-E-RABBY: *Quantification of the effect of tool geometric features on aspects of friction stir welding*, Ph. D. Thesis, College of Engineering and Computing, University of South Carolina, 2015.

[16] M. ASSIDI, L. FOURMENT, S. GUERDOUX and T. NELSON: 'Friction model for friction stir welding process simulation: Calibrations from welding experiments', *International Journal of Machine Tools and Manufacture*, Vol. 50, pp. 143-155, 2010.